Elasticity of Prussian blue analogue nanoparticles

Gautier Félix,[a] Mirko Mikolasek,[b] Helena J. Shepherd,[c] Jérôme Long,[a] Joulia Larionova,[a] Yannick Guari,[a] Jean-Paul Itié,[d] Aleksandr I. Chumakov,[b] William Nicolazzi,[e] Gábor Molnár,[e] and Azzedine Bousseksou*[e]

Abstract: We report on the elastic properties of Ni/$[Fe(CN)_6]$ Prussian blue analogue nanoparticles investigated by high pressure synchrotron X-ray diffraction and nuclear inelastic scattering. For 3 nm vs. 115 nm particles, we have obtained a bulk modulus of 30.3 ± 3.8 GPa vs. 24.5 ± 3.2 GPa, and a Debye sound velocity of 2496 ± 46 $m.s^{-1}$ vs. 2407 ± 38 $m.s^{-1}$, respectively. Combining these results, the Poisson's ratio, the Young's modulus, the shear modulus and the transversal/longitudinal sound velocities have been calculated. All these physical quantities suggest a stiffening of the lattice when decreasing the particle size, which is mainly attributed to the reduction of iron ions on the particle surface.

Introduction

Prussian blue analogues (PBA) are a broad family of face-centered cubic coordination networks, composed by a pair of transition metal ions connected by cyano bridges of general formula: $A_{1-x}N^{II}[M^{III}(CN)_6]_{1-x/3}$, (with A = alkaline ion, N and M the transition metal ions). The different combinations of metallic ions (and electronic configurations) allow different physico-chemical properties to be obtained, while keeping the same framework structure. Notably, certain PBA materials can display interesting ferromagnetic behavior[1-4] or electronic phase change phenomena, such as spin state switching[5,6] and Jahn-Teller switching,[7,8] which are – in most cases – induced by an inter-valence charge transfer between the metal ions. These electronic phenomena have received much attention as they are accompanied by a spectacular change of magnetic and optical properties.[9,10]

Due to the strong electron – lattice coupling, electronic phase transitions in PBA solids are governed to a large extent by the lattice properties. Of particular interest is the substantial change of lattice volume between the two states, which has been extensively investigated by powder X-ray diffraction methods under different external stimuli (temperature, pressure, light irradiation, ...).[5,6,11,12] On the other hand, the elastic properties of PBA materials remain much less explored: only a few bulk modulus measurements have been reported in the literature. By means of high pressure crystallographic methods, Bleuzen *et al.* have measured a bulk modulus of 43 ± 2 GPa for photomagnetic CoFe PBA materials,[11] while Pajerowski *et al.* obtained ca. 31 GPa for ferromagnetic NiCr PBA materials.[13] On the other hand, Boudkeddaden *et al.* have estimated the bulk moduli of B_{LT} = 30 ± 3 GPa and B_{HT} = 23 ± 2 GPa for the switchable PBA compound $RbMn[Fe(CN)_6]$ in the low and high temperature phases, respectively.[14] These data are particularly important to better understand the effect of an external pressure on the phase stability and also to rationalize the elastic energy changes, which accompany the phase transitions in PBA materials.[15] The in-depth knowledge of the elastic properties of PBA compounds is also an asset for their possible future applications in mechanical actuators (using the volume change).[16]

Besides bulk PBA compounds, more recently, the development of PBA nano-objects has led to the observation of new physical phenomena in this class of nanomaterials, such as superparamagnetism.[17,18] Core@shell particles such as PBA@PBA and Au@PBA heterostructures with original magnetic[19-22] and optical[23] properties have been also synthesized. These heterostructures exhibit in many cases mechanical strain-mediated coupling between the electronic and magnetic properties of the core and the shell. When one of the components undergoes an electronic phase transition this coupling can even allow the switching of the properties of the second component.[22,24] Theoretical analysis highlighted that the pressure that the core (shell) can apply to the shell (core) upon the phase transition can be estimated if the Young's moduli and Poisson's ratio of both components are known.[25] Then, combining the theoretical prediction and a synthetic control of the core and shell thickness, the applied pressure on the core and the shell could be controlled, opening the way to monitor the synergy between magnetism, optical and electronic phenomena in PBA heterostructures. However, the elastic properties of nanoscale PBA materials remain completely unknown. To go further in the understanding of the mechanical properties of these materials (both bulk and nanoscale) the determination of elastic coefficients becomes thus indispensable.

In a previous work, using Mössbauer spectroscopy we analyzed the evolution of lattice stiffness as a function of the particle size in $Ni^{II}/[Fe^{III}(CN)_6]$ nanoparticles and revealed a stiffening of the lattice for ultra-small particles (ca. 3 nm), reflected by the increase of their Debye temperature Θ_D.[26] Based on Raman and FTIR spectroscopy data this stiffening was attributed to a reduction of the ferric ions on the surface of the particles. In the present work, we combined high pressure synchrotron x-ray diffraction (XRD) and nuclear inelastic scattering (NIS) methods to determine the bulk modulus B and the Debye sound velocity v_D for 3 nm and 115 nm Ni/$[Fe(CN)_6]$ nanoparticles. Using these data we were able to calculate the Young's modulus Y, shear modulus G, Poisson's ratio v and the transversal/longitudinal sound velocities (v_t, v_l).

[a] Dr. G. Félix, Dr. J. Long, Prof. J. Larionova, Dr. Y. Guari
Institut Charles Gerhardt Montpellier, UMR 5253, Ingénierie Moléculaire et Nano-Objets, Université de Montpellier, ENSCM, CNRS, Place E. Bataillon, 34095 Montpellier Cedex 5, France.
[b] Dr. M. Mikolasek, Dr. A. I. Chumakov
ESRF-The European Synchrotron, CS40220, 38043 Grenoble Cedex 9, France
[c] Dr. H. J. Shepherd
School of Physical Sciences, University of Kent, Park Wood Rd, Canterbury CT2 7NH, United Kingdom
[d] Dr. J.-P. Itié
Synchrotron SOLEIL, L'Orme des Merisiers, Saint-Aubin, 91192 Gif-sur-Yvette, France
[e] Dr. W. Nicolazzi, Dr. G. Molnár, Dr. A. Bousseksou
Laboratoire de Chimie de Coordination, CNRS & Université de Toulouse (UPS, INP), 205 route de Narbonne 31077 Toulouse, France
E-mail: azzedine.bousseksou@lcc-toulouse.fr

Additionally, we have also confirmed the surface reduction in the case of 3 nm nanoparticles.

Results and Discussion

PBA nanoparticles were synthesized using previously reported methods. The smallest nanoparticles (3 nm) were obtained in the presence of a stabilizing agent (Poly(ethylene glycol) bis(3-aminopropyl), PEG-NH_2) during the synthesis, while the larger nanoparticles were obtained from the controlled precipitation of Ni^{2+} and $[Fe(CN)_6]^{3-}$ moieties wherein the increasing concentration and addition rate leads to an increase of the nanoparticle size. The resulting nanoparticles were post-synthetically functionalized by the PEG-NH_2 stabilizer.[26]

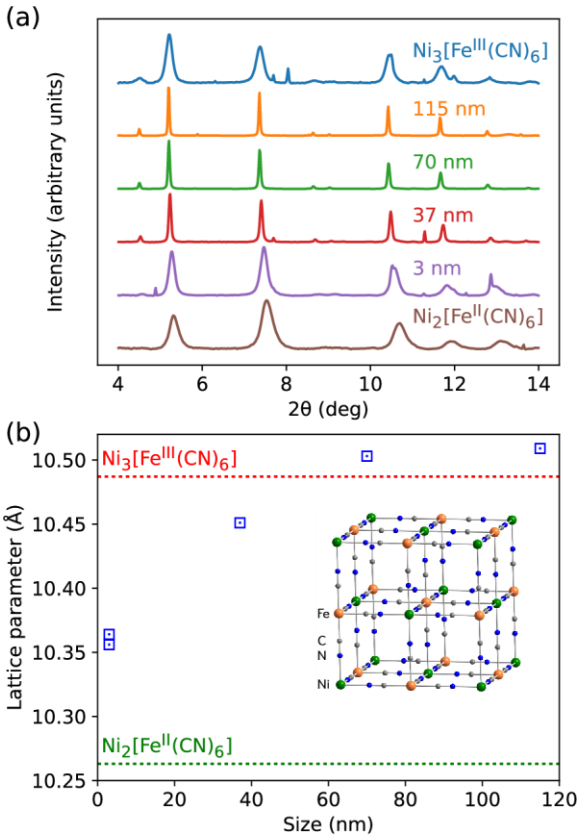

Figure 1. (a) Synchrotron x-ray diffraction patterns of Ni/$[Fe(CN)_6]$ measured at room temperature in the 2θ interval 4°–14° (λ = 0.477 Å), for different sizes of nanoparticles. (b) Lattice parameter of Ni/$[Fe(CN)_6]$ particles as a function of their size (the cubic structure is shown in the insert). The dashed lines represent the lattice parameters of the bulk $Ni_3[Fe^{III}(CN)_6]_2$ and $Ni_2[Fe^{II}(CN)_6]$ materials.

Figure 1 (a) shows synchrotron X-ray diffraction patterns for different sizes of Ni/$[Fe(CN)_6]$ nanoparticles, and for two bulk materials $Ni_3[Fe^{III}(CN)_6]_2$ and $Ni_2[Fe^{II}(CN)_6]$. The intense peaks at 5.2° and 7.4° correspond, respectively, to the (200) and (220) reflections of the well-known face-centered cubic structure[27,28] (see insert of Figure 1 (b)). It is interesting to note that for the largest nanoparticles (115 nm, 70 nm, 37 nm) the width of the diffraction peaks is narrower than in the bulk materials - due most likely to some disorder in these latter. Usually, larger peaks are expected when decreasing the size (*cf.* Scherer equation). This phenomenon is observed for the nanoparticles. We explain the unusual behavior of bulk materials by the difference between bulk and nanoparticles in synthesis procedures, which can introduce different kind of defect in the crystal structures.

The cell parameter *a* of the Prussian blue cubic lattice was then calculated using the position of the (200) reflections. Figure 1 (b) shows the evolution of *a* as a function of the particle size. The cell parameters of the two bulk compounds ($Ni_3[Fe^{III}(CN)_6]_2$ and $Ni_2[Fe^{II}(CN)_6]$) are also shown. As it can be expected the density of the bulk $Ni_2[Fe^{II}(CN)_6]$ material is substantially higher than that of the bulk $Ni_3[Fe^{III}(CN)_6]_2$. The cell parameters of the 115 nm and 70 nm particles are similar (slightly higher) when compared to the bulk $Ni_3[Fe^{III}(CN)_6]_2$. When decreasing the size, the cell parameter decreases also. Using the Mössbauer spectrum of the 3 nm (resp. 37 nm)[26] particles, we obtain a percentage of 85 ± 7 % (resp. 10 ± 17 %) and 15 ± 7 % (resp. 90 ± 20 %) for the Fe^{II} and Fe^{III} species, respectively. Then, at 3 nm the influence of the reduced species Fe^{II}-CN-Ni^{II} on the surface is dominant, which leads to a cell parameter approaching that of the bulk $Ni_2[Fe^{II}(CN)_6]$ material.

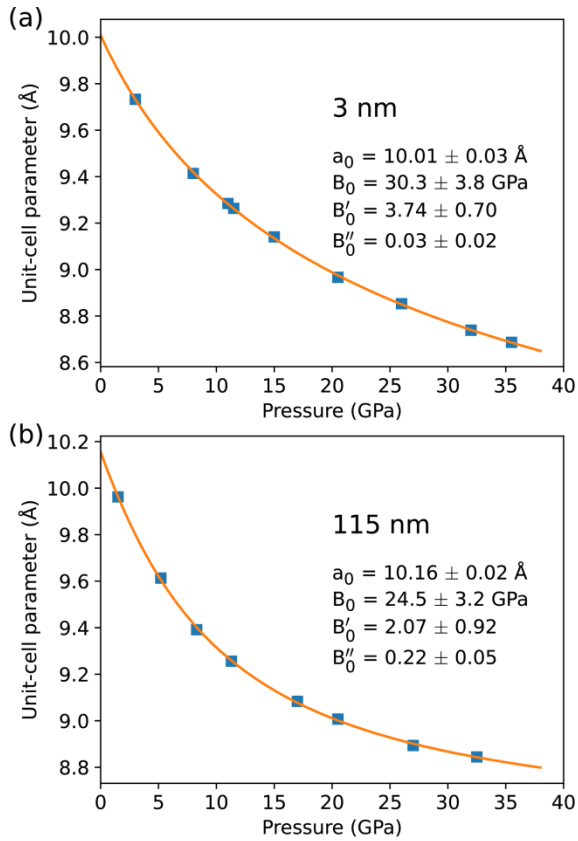

Figure 2. Evolution of the unit cell parameter as a function of the pressure for the 3nm (a) and 115nm (b) particles. The squares and lines represent, respectively, the experimental data and the fits using equations (1) and (3). The fitted parameters are displayed in insert of each graph.

In order to get further insights into their elastic properties, the 3 nm and 115 nm samples were further investigated using high pressure XRD. It may be worth to note that the diffractograms in Figure 1 (a) were recorded in a liquid (methanol/ethanol/water) medium. However, when applying pressure to this mixture the

lattice parameters of the PBA samples evolved in an 'anomalous' manner, probably due to a structural phase transition mediated by the strong physico-chemical interactions between the particles and the liquid. We have not investigated in detail this phenomenon, but changed to a more inert pressure transmitting medium (neon) which was then successfully used to apply hydrostatic pressures up to 35 GPa (at room temperature) on our samples. The evolution of the cell parameters as a function of the pressure are displayed in Figures 2 (a) and (b) for the 3 nm and 115 nm samples, respectively. The unit cell parameter *a* was calculated in both case using the (200) reflection. (*N.B.* The differences in the unit cell parameters between the results in Figures 1 and 2 arise most likely due to the different sample environments.) From these measurements, we have extracted the bulk modulus of the particles using the 2nd order Murnaghan approximation for the bulk modulus:[29]

$$B(P) = B_0 + B_0'P + B_0''P^2 \qquad (1)$$

with B_0 the bulk modulus at zero pressure, and B_0' and B_0'' the first and second order constants of the bulk modulus, respectively. The second order approximation was used because a simple approximation of a linear evolution of the bulk modulus as a function of the pressure was not satisfactory (B_0'' is not negligible). Taking into account the general definition of the bulk modulus (inverse of compressibility χ_T):

$$\chi_T = \frac{1}{B(P)} = -\frac{1}{V}\left(\frac{\partial V}{\partial P}\right)_T \qquad (2)$$

The evolution of the unit cell parameter of a cubic lattice as a function of the pressure can be written as follows:

$$a(P) = a_0 \exp\left(-\int_0^P \frac{\mathrm{d}P}{3B(P)}\right) \qquad (3)$$

with a_0 the cell parameter at zero pressure. Using equations (1) and (3), we found a bulk modulus of 30.3 ± 3.8 GPa and 24.4 ± 3.2 GPa for the 3 nm and 115 nm particles, respectively. This result is in good agreement with our previous Mössbauer spectroscopic investigation,[26] which indicated that the stiffness of the NiFe PBA nanoparticles increases with decreasing the size.

To fully characterize the elastic properties of the 3 nm and 115 nm samples, we have determined further lattice dynamical parameters using the nuclear inelastic scattering technique (NIS). NIS spectra were collected for 3 nm and 115 nm particle sizes and treated as described in ref. [30], in order to finally obtain the iron vibrational density of states (DOS) of Ni/[Fe(CN)$_6$] nanoparticles (Figure 3 (a)). In the present work, the powder form of the samples implies an iron-partial DOS averaged over all directions of phonon polarizations (i.e. over all directions of atomic displacements).

Several modes can be identified by means of the composition factor[31,32] which is derived from the selection rules of the NIS. In randomly oriented powder, the composition factor e_j^2 (with $\mathbf{e}_j$ the polarization vector) is directly related to the fraction $\tilde{g}_j$ of DOS such as:

$$\tilde{g}_j = \int_{E_{j,1}}^{E_{j,2}} \tilde{g}\,(E)dE = \frac{1}{3}e_j^2 \qquad (4)$$

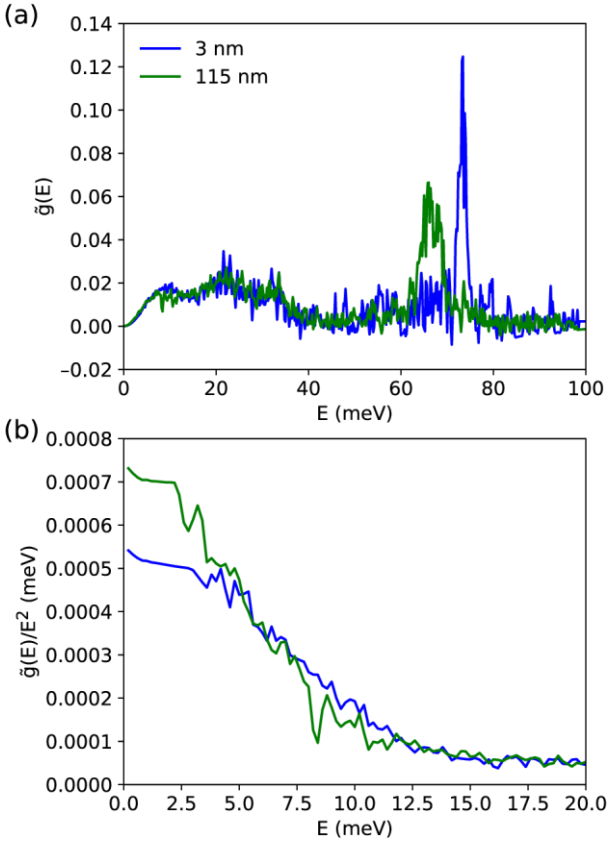

Figure 3. (a) Iron-DOS $\tilde{g}$ (E) of Ni/[Fe(CN)$_6$] for the 3 nm and 115 nm nanoparticle samples. (b) $\tilde{g}$/E^2 in the low energy range (acoustic modes) for the two samples.

By assuming a total decoupling of inter- and intramolecular vibrations, the upper limit of the composition factor for each acoustic branch can be written as:

$$e_{ac}^2 = \tilde{m}/M_\Sigma \qquad (5)$$

where $\tilde{m}$ is the mass of the resonant atoms in the cell and M_Σ is the mass of the primitive cell (1/4 of the mass of the chosen conventional face-centred cubic cell). Considering the three acoustic modes, the limit of the acoustic part E_{ac} can be estimated as:

$$\int_0^{E_{ac}} \tilde{g}\,(E)dE \approx 3 \cdot \frac{1}{3}e_{ac}^2 = 0.21 \qquad (6)$$

The estimated upper acoustic limit $E_{ac} \approx 18$ meV is roughly the same for both the 3 nm and 115 nm particles. The first peak in the DOS around ~ 8-12 meV is thus composed of acoustic modes, while the broad peaks around ~ 23 meV and ~ 33 meV are due to optical branches.

In the same way, using the composition factor, it is possible to identify stretching modes of the Fe coordination octahedron. In the case of the 115 nm particles, the well-defined optical mode at 66 meV corresponds probably to the three-fold degenerated F_{1u} stretching modes of the perfect octahedron. In this case, by assuming the stretching of two rigid fragments, with respective masses M_1 and M_2, and that the resonant atom belongs to the fragment with mass M_1, the composition factor for each mode can be written as:

$$e_{opt}^2 = \frac{\tilde{m}\, M_2}{M_1(M_1+M_2)} = \frac{\tilde{m}\,(M_\Sigma - M_1)}{M_1 M_\Sigma} \qquad (7)$$

The composition factor has been determined fitting the peak with a pseudo-Voigt function and by integrating it as described by equation (4). By using equation (7) and taking into account the three-fold degeneracy of the mode, the fragment mass of the resonant atom is estimated as $M_1 = 107$ a.u., which is in good agreement with the expected fragment mass associated with one iron atom and two CN groups (109 a.u.). Therefore, this mode can be clearly identified as the threefold degenerated stretching of the iron ion with two CN groups in the local environment. In the case of the 3 nm particles, the same peak is located around 73 meV due to the reduction of iron ions on the surface. Indeed, this reduction leads to a decrease of the Fe–C bond length, which is associated with a stiffening of the bond, leading to the upshift of the peak. This result confirms our previous observations of a chemical reduction $Ni^{II}/[Fe^{III}(CN)_6] \rightarrow Ni^{II}/[Fe^{II}(CN)_6]$ at the surface of the particles, evidenced by Raman, infra-red and Mössbauer spectroscopies.[26] By determining the composition factor, the fragment mass is calculated at $M_1 = 130$ a.u., which is larger than for the 115 nm particles. This can be explained by (i) an increase of the fragment mass M_1, (ii) a decrease of the primitive cell mass which leads to an overestimation of M_Σ or (iii) the presence of an additional vibrational mode in the peak area. The first explanation is unlikely and can be excluded. The second is possible if a decrease of the averaged mass of the primitive cell due to the strong contribution of the surface (incomplete cell on the surfaces due to the breaking of the periodicity) is considered. The third is the most likely due to the fact that each optical mode does not present a similar shift due to the surface reduction. It can lead to the superimposition of several peaks and thus to an increase of the composition factor which is proportional to the area under the curve.

Table 1. Main lattice dynamical parameters extracted from the NIS spectra.

$Ni_3[Fe(CN)_6]_2$		3 nm	115 nm
Lamb-Mössbauer factor	f_{LM}	0.58(1)	0.555(1)
Vibrational amplitude (Å)	$\sqrt{\langle x_{Fe}^2 \rangle}$	0.176(8)	0.184(2)
Mean force constant (N/m)	$\langle C_{Fe} \rangle$	587(15)	502(10)
Internal energy per atom (meV)	$u_{vib,N}$	100(1)	97.0(1)
Entropy per atom (k_B)	$s_{vib,N}$	2.57(8)	2.65(2)
Specific heat (k_B)	C_V	2.26(8)	2.33(2)

Table 1 summarizes some relevant lattice dynamical parameters extracted from the DOS following the methods described in ref. [33]. The Lamb-Mössbauer factor, the vibrational amplitude and the mean force constant show the same trend: an increase of lattice stiffness upon size diminution. The vibrational internal energy tends to be higher for stronger bonds, while a decrease of the vibrational entropy is observed.

The Debye sound velocity v_D can be also extracted from the extrapolation of the DOS at E = 0 meV, using the Debye model such as:[34,35]

$$\lim_{E\to 0} \tilde{g}(E) \approx \tilde{g}_D(E) = \frac{\tilde{m}}{2\pi^2 \rho \hbar^3 v_D^3} E^2 \qquad (8)$$

where $\tilde{g}_D$, $\tilde{m}$, ρ and ħ are the DOS in the Debye model, the mass of the resonant atom (^{57}Fe), the volumetric mass density of $Ni_3[Fe(CN)_6]_2$ and the reduced Planck constant, respectively. In practice, v_D was extracted using figure 3 (b). The sound velocity for the 115 and 3 nm particles are $v_{D,115\mathrm{nm}}$ = 2407 ± 38 m.s^{-1} and $v_{D,3\mathrm{nm}}$ = 2496 ± 46 m.s^{-1}, respectively. In the approximation of an isotropic material, the Debye sound velocity is directly related to the Young's modulus Y and the Poisson's ratio ν by the following relationships:[30]

$$Y = h_1(\nu)\rho v_D^2 = \left(\frac{2\alpha+\beta}{3}\right)^{\frac{2}{3}} \rho v_D^2 \qquad (9)$$

where $h_1(\nu)$ is a function which depends only on ν, with

$$\alpha = [2(1+\nu)]^{\frac{3}{2}} \qquad (10)$$

and

$$\beta = \left[\frac{(1-2\nu)(1+\nu)}{1-\nu}\right]^{\frac{3}{2}} \qquad (11)$$

From this point, the bulk modulus B can be also calculated as:

$$B = \frac{Y}{3(1-2\nu)} = \frac{h_1(\nu)}{3(1-2\nu)} \cdot \rho v_D^2 \qquad (12)$$

Therefore, using the bulk modulus data from high pressure XRD and the Debye sound velocity data from NIS, the Poisson's ratio for the 115 nm and 3 nm particles can be determined as $\nu_{115\mathrm{nm}}$ = 0.352 ± 0.023 and $\nu_{3\mathrm{nm}}$ = 0.365 ± 0.021, respectively. Using the Poisson's ratio, the Young's modulus was properly obtained for the two sizes as $Y_{115\mathrm{nm}}$ = 21.3 ± 1 GPa and $Y_{3\mathrm{nm}}$ = 24.1 ± 1.2 GPa. The shear modulus G can also be calculated, using the following equation:

$$G = \frac{Y}{2(1+\nu)} \qquad (13)$$

The calculated shear moduli of the 115 nm and 3 nm particles are $G_{115\mathrm{nm}}$ = 7.9 ± 0.5 GPa and $G_{3\mathrm{nm}}$ = 8.8 ± 0.6 GPa, respectively. Finally, the transversal v_t and longitudinal v_l sound velocities can be calculated such as:

$$v_t = \sqrt{\frac{G}{\rho}} = \sqrt{\frac{Y}{\rho}} \cdot \sqrt{\frac{1}{2(1+\nu)}} \qquad (14)$$

$$v_l = \sqrt{\frac{Y}{\rho}} \cdot \sqrt{\frac{1-\nu}{(1+\nu)(1-2\nu)}} \qquad (15)$$

The various elastic moduli for the two particle sizes are summarized in table 2. It may be worth to note also that due to the isotropic nature of the lattice, it is not necessary to characterize the elastic moduli in all directions of the space.

Overall the results in Table 2 are consistent with the XRD patterns, which describe a change of the density with the size, but a conservation of the face centered structure. The different measurements and extracted parameters show in a coherent way that the size reduction indeed affects the elastic properties of the nanoparticles. While the lattice stiffening in the small particles can be deduced from the increase of the Debye temperature (Mössbauer spectroscopy) and the bulk modulus (XRD), the differences remain comparable with the error bars. On the other hand, the sound velocity (NIS) and the calculated Young's modulus and shear modulus data confirm this trend of lattice stiffening without overlap of errors. The Poisson's ratio does not give information about the stiffness, but rather the relation between the Young's, bulk and shear moduli. The observed values (0.35-36) can be considered as typical for inorganic crystalline materials.

Table 2. Elastic properties of PBA nanoparticles.

$Ni_3[Fe(CN)_6]_2$		3 nm	115 nm
Debye temperature (K)[18]	θ_D	225 ± 15	187 ± 12
Young's modulus (GPa)	Y	24.1 ± 1.2	21.3 ± 1
Bulk modulus (GPa)	B	30.3 ± 3.8	24.5 ± 3.2
Shear modulus (GPa)	G	8.8 ± 0.6	7.9 ± 0.5
Poisson's ratio	ν	0.365 ± 0.021	0.352 ± 0.023
Debye sound velocity ($m.s^{-1}$)	v_D	2496 ± 46	2407 ± 38
Transversal sound velocity ($m.s^{-1}$)	v_t	2216 ± 34	2140 ± 27
Longitudinal sound velocity ($m.s^{-1}$)	v_l	4806 ± 369	4489 ± 326

Conclusions

To summarize, high pressure XRD and NIS have allowed the size dependence of both the structure and the vibrational density of states to be followed for Ni/$[Fe(CN)_6]$ particles. These data were used to extract lattice dynamical parameters, such as vibration amplitude, mean force constants or vibrational entropy and internal energy, and to determine the elastic moduli (bulk, Young's and shear moduli) as well as the Poisson's ratio. We have shown that the chemical reduction at the surface of the smallest nanoparticles leads to a diminution of the lattice parameter as well as to a shift to higher energies of the metal-ligand stretching mode. This contributes to an increase of the global stiffness of the smallest particles, which is characterized by an increase of all the elastic parameters (v_D, B, Y, G and ν). Access to the elastic moduli of PBA nanoparticles, which are largely unknown in molecule-based materials (bulk and nano-object), is of paramount importance for developing applications based on the mechanical properties of molecular materials, such as micro-electromechanical system (MEMS)[36,37] or mechanically-coupled nano-heterostructures.[22,38] It is important to stress also that in this work, we provide an accurate value of the Poisson's ratio. The mechanical characterization of coordination networks is challenging, especially at the nanoscale, but necessary for the development of new applications. In this context, high pressure XRD and NIS appear as suitable techniques, which overcome the usual restrictions of the other methods.

Experimental Section

The synthesis of the samples was described in Ref [26]. The synchrotron powder x-ray diffraction experiments were carried out at PSICHÉ-SOLEIL and PETRA III-DESY beamlines. The samples were placed in diamond anvil cells and the pressure was measured using the ruby fluorescence technique. At PSICHÉ-SOLEIL, the pressure transmitter medium was water-ethanol-methanol liquid and the used beam wavelength was λ=0.477 Å. At PETRA III-DESY, the pressure transmitter medium was neon gas and the used beam wavelength was λ=0.29056 Å. NIS experiments were performed at the Nuclear Resonance beamline ID18[39] at the European Synchrotron Radiation Facility (ESRF, Grenoble) in the hybrid bunch modes at room temperature, using non enriched samples with natural ^{57}Fe.

Acknowledgements

The authors would like to thank the financial support from the Agence Nationale de la Recherche (NANOHYBRID project, ANR-13-BS07-0020-01) and from the Federal University of Toulouse (project IDEX Emergence NEMSCOOP). We are indebted to Leonid Dubrovinsky (Bayerisches Geoinstitut) for his kind help.

Keywords: Prussian blue analogues • Nanoparticles • Elastic properties • X-ray diffraction • Mössbauer spectroscopy

[1] W. R. Entley, G. S. Girolami, *Science* **1995**, *268*, 397–400
[2] S. Ferlay, T. Mallah, R. Ouahès, P. Veillet, M. Verdaguer, *Nature* **1995**, *378*, 701–703
[3] O. Sato, T. Iyoda, A. Fujishima, K. Hashimoto, *Science* **1996**, *272*, 704–705
[4] M. Verdaguer, A. Bleuzen, V. Marvaud, J. Vaissermann, M. Seuleiman, C. Desplanches, A. Scuiller, C. Train, R. Garde, G. Gelly, C. Lomenech, I. Rosenman, P. Veillet, C. Cartier, F. Villain, *Coord. Chem. Rev.* **1999**, *190192*, 1023–1047
[5] N. Shimamoto, S.-i. Ohkoshi, O. Sato, K. Hashimoto, *Inorg. Chem.* **2002**, *41*, 678–684
[6] W. Kosaka, K. Nomura, K. Hashimoto, S.-i. Ohkoshi, *J. Am. Chem. Soc.* **2005**, *127*, 8590–8591
[7] S.-i. Ohkoshi, H. Tokoro, K. Hashimoto, *Coordination Chemistry Reviews* **2005**, *249*, 1830–1840
[8] T. Mahfoud, G. Molnár, S. Bonhommeau, S. Cobo, L. Salmon, P. Demont, H. Tokoro, S.-I. Ohkoshi, K. Boukheddaden, A. Bousseksou, *J. Am. Chem. Soc.* **2009**, *131*, 15049–15054
[9] V. Ksenofontov, G. Levchenko, S. Reiman, P. Gütlich, A. Bleuzen, V. Escax, M. Verdaguer, *Phys. Rev. B* **2003**, *68*, 024415
[10] H. Tokoro, T. Matsuda, K. Hashimoto, S.-i. Ohkoshi, *J App. Phys.* **2005**, *97*, 10M508
[11] A. Bleuzen, J.-D. Cafun, A. Bachschmidt, M. Verdaguer, P. Münsch, F. Baudelet, J.-P. Itié, *J. Phys. Chem. C* **2008**, *112*, 17709–17715
[12] V. Escax, A. Bleuzen, J. P. Itié, P. Munsch, F. Varret, M. Verdaguer, *J. Phys. Chem. B* **2003**, *107*, 4763–4767
[13] D. M. Pajerowski, S. E. Conklin, J. Leão, L. W. Harriger, D. Phelan, *Phys. Rev. B* **2015**, *91*, 094104
[14] K. Boukheddaden, E. D. Loutete-Dangui, E. Codjovi, M. Castro, J. A. Rodriguéz-Velamazán, S. Ohkoshi, H. Tokoro, M. Koubaa, Y. Abid, F. Varret, *J. Appl. Phys.* **2011**, *109*, 013520
[15] H. Spiering, K. Boukheddaden, J. Linares, F. Varret, *Phys. Rev. B* **2004**, *70*, 184106
[16] H. J. Shepherd, I. A. Guralskiy, C. M. Quintero, S. Tricard, L. Salmon, G. Molnár, A. Bousseksou, *Nat. Commun.* **2013**, *4*, 2607
[17] L. Catala, T. Gacoin, J.-P. Boilot, É. Rivière, C. Paulsen, E. Lhotel, T. Mallah, *Adv. Mater.* **2003**, *15*, 826–829
[18] W. Kosaka, M. Tozawa, K. Hashimoto, S.-i. Ohkoshi, *Inorg. Chem. Commun.* **2006**, *9*, 920–922
[19] Y. Prado, N. Dia, L. Lisnard, G. Rogez, F. Brisset, L. Catala, T. Mallah, *Chem. Comm.* **2012**, *48*, 11455–11457
[20] M. F. Dumont, E. S. Knowles, A. Guiet, D. M. Pajerowski, A. Gomez, S. W. Kycia, M. W. Meisel, D. R. Talham, *Inorg. Chem.* **2011**, *50*, 4295–4300

[21] N. Dia, L. Lisnard, Y. Prado, A. Gloter, O. Stéphan, F. Brisset, H. Hafez, Z. Saad, C. Mathonière, L. Catala, T. Mallah, *Inorg. Chem.* **2013**, *52*, 10264–10274

[22] O. N. Risset, P. A. Quintero, T. V. Brinzari, M. J. Andrus, M. W. Lufaso, M. W. Meisel, D. R. Talham, *J. Am. Chem. Soc.* **2014**, *136*, 15660–15669

[23] G. Maurin-Pasturel, J. Long, Y. Guari, F. Godiard, M.-G. Willinger, C. Guerin, J. Larionova, *Angew. Chem. Int. Ed.* **2014**, *53*, 3872–3876

[24] M. Presle, I. Maurin, F. Maroun, R. Cortès, L. Lu, R. Sayed Hassan, E. Larquet, J.-M. Guigner, E. Rivière, J. P. Wright, J.-P. Boilot, T. Gacoin, *J. Phys. Chem. C* **2014**, *118*, 13186–13195

[25] G. Félix, M. Mikolasek, G. Molnár, W. Nicolazzi, A. Bousseksou, *Eur. J. Inorg. Chem.* **2017**, DOI: 10.1002/ejic.201700121

[26] G. Félix, W. Nicolazzi, L. Salmon, G. Molnár, M. Perrier, G. Maurin, J. Larionova, J. Long, Y. Guari, A. Bousseksou, *Phys. Rev. Lett.* **2013**, *110*, 235701

[27] H. J. Buser, D. Schwarzenbach, W. Petter, A. Ludi, *Inorg. Chem.* **1977**, *16*, 2704–2710

[28] Y. Mizuno, M. Okubo, K. Kagesawa, D. Asakura, T. Kudo, H. Zhou, K. Oh-ishi, A. Okazawa, N. Kojima, *Inorg. Chem.* **2012**, *51*, 10311–10316

[29] L. M. Thomas, J. Shanker, *phys. stat. sol. (b)* **1995**, *189*, 363–369

[30] G. Félix, M. Mikolasek, H. Peng, W. Nicolazzi, G. Molnár, A. I. Chumakov, L. Salmon, A. Bousseksou, *Phys. Rev. B* **2015**, *91*, 024422

[31] J. T. Sage, S. M. Durbin, W. Sturhahn, D. C. Wharton, P. M. Champion, P. Hession, J. Sutter, E. E. Alp, *Phys. Rev. Lett.* **2001**, *86*, 4966–4969

[32] A. I. Chumakov, R. Rüffer, O. Leupold, I. Sergueev, *Struct. Chem.* **2003**, *14*, 109–119

[33] A. I. Chumakov, W. Sturhahn, *Hyperfine Interact.* **1999**, *123-124*, 781–808

[34] K. Achterhold, C. Keppler, A. Ostermann, U. van Bürck, W. Sturhahn, E. E. Alp, F. G. Parak, *Phys. Rev. E* **2002**, *65*, 051916

[35] M. Y. Hu, W. Sturhahn, T. S. Toellner, P. D. Mannheim, D. E. Brown, J. Zhao, E. E. Alp, *Phys. Rev. B* **2003**, *67*, 094304

[36] M. D. Manrique-Juárez, S. Rat, L. Salmon, G. Molnár, C. M. Quintero, L. Nicu, H. J. Shepherd, A. Bousseksou, *Coord. Chem. Rev.* **2016**, *308, Part 2*, 395–408

[37] M. D. Manrique-Juarez, F. Mathieu, V. Shalabaeva, J. Cacheux, S. Rat, L. Nicu, T. Leïchlé, L. Salmon, G. Molnár, A. Bousseksou, *Angew. Chem. Int. Ed.* **2017**, DOI: 10.1002/anie.201702739

[38] A. C. Felts, M. J. Andrus, E. S. Knowles, P. A. Quintero, A. R. Ahir, O. N. Risset, C. H. Li, I. Maurin, G. J. Halder, K. A. Abboud, M. W. Meisel, D. R. Talham, *J Phys. Chem. C* **2016**, *120*, 5420–5429

[39] R. Rüffer, A. I. Chumakov, *Hyperfine Interact.* **1996**, *97-98*, 589–604

Entry for the Table of Contents

COMMUNICATION

The elastic behavior of Prussian blue analogue nanoparticles has been investigated, using high pressure synchrotron X-ray diffraction and nuclear inelastic scattering techniques. We succeed to extract all elastic moduli for different sizes of Prussian blue analogue nanoparticles. This result is determinant for the understanding of electron-lattice coupling phase transition at the nanoscale.

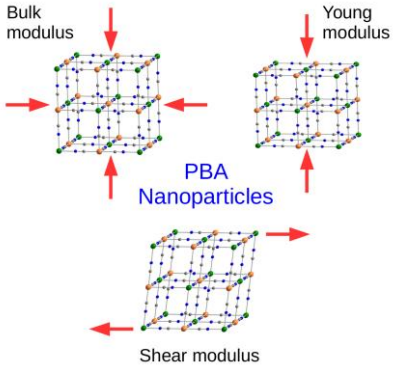

Prussian Blue analogues*

*Gautier Félix, Mirko Mikolasek, Helena J. Shepherd, Jérôme Long, Joulia Larionova, Yannick Guari, Jean-Paul Itié, Aleksandr I. Chumakov, William Nicolazzi, Gábor Molnár, and Azzedine Bousseksou**

Page No. – Page No.

Elasticity of Prussian blue analogue nanoparticles

*one or two words that highlight the emphasis of the paper or the field of the study